Journal of Materials Chemistry

Cite this: *J. Mater. Chem.*, 2012, **22**, 5155

www.rsc.org/materials

PAPER

Composite silica nanospheres covalently anchored with gold nanoparticles at the outer periphery of thermoresponsive polymer brushes†

Tao Wu, Qianqian Zhang, Jinming Hu, Guoying Zhang* and Shiyong Liu*

Received 29th October 2011, Accepted 3rd January 2012
DOI: 10.1039/c2jm15530c

We report on the fabrication of water-dispersible composite silica nanospheres covalently anchored with gold nanoparticles (AuNPs) possessing thermo-tunable spatial distributions at the outer periphery of thermoresponsive poly(*N*-isopropylacrylamide) (PNIPAM) brushes. Starting from initiator-functionalized silica nanoparticles, surface-initiated atom transfer radical polymerization (ATRP) of *N*-isopropylacrylamide (NIPAM) afforded hybrid silica nanoparticles coated with PNIPAM brushes. The substitution reaction of halogen terminal groups of grafted PNIPAM chains with sodium azide and subsequent click reaction with 1,2-dithiolane-3-pentanoic acid-*N*-propargylamide afforded hybrid silica nanoparticles coated with 1,2-dithiolane end-capped PNIPAM brushes. AuNPs were then covalently anchored to the outer periphery of hybrid silica nanoparticles by utilizing strong chemisorption of surface-attached dithiolane moieties to AuNPs. Dynamic laser light scattering (LLS) measurements revealed that thermosensitive PNIPAM brushes at the surface of hybrid silica nanoparticles exhibit reversible thermo-induced collapse/swelling transitions, leading to the facile thermo-modulation of spatial distributions of AuNPs covalently attached at the periphery of composite silica nanospheres and thermo-reversible surface plasmon absorption band shift. The reported strategy of covalent assembly of AuNPs into well-defined composite nanospheres possessing thermo-tunable characteristics might be further exploited for colorimetric temperature sensing and responsive SERS detection purposes.

1. Introduction

The unique physical properties of metallic and inorganic nanoparticles have rendered them to be the main driving force of nanotechnology development, offering tremendous scope for their next-generation biomedical applications such as drug delivery, cell and tissue imaging, biosensing, and disease diagnosis.[1,2] On the other hand, clusters or controlled assemblies of metallic and inorganic nanoparticles have recently been recognized as a key impetus to enhance the relevant physical properties and cooperative functions, as compared to single nanoparticles.[3–6] For example, controlled self-assembly of gold nanoparticles (AuNPs) has been thoroughly explored and scrutinized for enhanced functions in diverse fields ranging from cancer photothermotherapy, cell imaging, sensors, optical detection, to catalysis.[6–13] Clusters of gold or silver nanoparticles can be employed for surface enhanced Raman scattering (SERS) signal amplification due to the presence of Raman hotspots from closely packed nanoparticles and the local electromagnetic coupling effect.[13–16] As for magnetic iron oxide nanoparticles, their secondary clusters exhibit improved magnetic resonance (MR) imaging contrast enhancement and considerably larger responses under external magnetic field biology, as compared to single magnetic nanoparticles.[17]

During the past decade, various strategies have been developed for the controlled assembly of AuNPs. Upon appropriate surface modification of AuNPs with small functional molecules, polymers, DNA, and proteins, the self-assembly of AuNPs can be achieved by taking advantage of noncovalent interactions including hydrogen bonding,[18–20] electrostatic interactions,[21–24] π–π interaction,[25,26] host–guest interaction[27–32] or a combination of them. Template-assisted self-assembly of AuNPs has also emerged to be a main strategy, starting from 1D, 2D, or 3D inorganic or organic templates with predetermined morphology and functional group distributions.[33–44] For example, the rich library of morphologies of block copolymer self-assemblies has also been exploited as a template for controlling the self-organization of AuNPs into well-defined clusters or aggregates.[33]

In addition to the fabrication of controlled assemblies of AuNPs, the facile and reversible modulation of interparticle distances after nanoparticle assemblies have formed is also highly

CAS Key Laboratory of Soft Matter Chemistry, Department of Polymer Science and Engineering, Hefei National Laboratory for Physical Sciences at the Microscale, University of Science and Technology of China, Hefei, Anhui 230026, China. E-mail: sliu@ustc.edu.cn; gyzhang@ustc.edu.cn

† Electronic supplementary information (ESI) available: Supplementary figs. S1–S2. See DOI: 10.1039/c2jm15530c

important, as it is directly relevant to the tuning of the collective optical, electrical, and magnetic properties of assembled AuNP clusters.[12,13,37,42–48] For instance, the decrease of interparticle distance within AuNP assemblies can enhance interparticle coupling, leading to the red-shift and broadening of the surface plasmon absorption band. These characteristics have been widely utilized for SERS detection, colorimetric sensors, and photothermotherapy.[6,11–13] In principle, the interparticle distance within AuNP assemblies can be modulated by tuning the chain length of stabilizing and/or interacting molecules anchored at the surface of AuNPs.[45–47] In the template-assisted AuNP assembly approach, the interparticle distance can be tuned by controlling the grafting density and distribution pattern of binding sites at the surface of templates.[43]

In most cases, once AuNP assemblies were formed, the spatial distribution of AuNP building blocks within the nanoparticle clusters has been fixed. Thus, it is highly desirable to fabricate responsive AuNP assemblies, of which the overall dimensions and interparticle spatial distances can respond and adapt to external stimuli.[49,50] In principle, this can be achieved by employing templates with responsive characteristics for AuNP assembly. Previously, stimuli-responsive polymeric nanogels and microgels, (cross-linked) micellar nanoparticles, star polymers, and core-shell type hybrid nanoparticles have been utilized to physically encapsulate AuNPs or as nanoreactors for the *in situ* formation of AuNP aggregates.[37,42,51–54] The spatial distribution of embedded AuNPs can be tuned to some extent upon appropriate external stimuli. However, the structural stability of templated nanoparticle assemblies is an issue due to unstable interactions between AuNPs and the template matrix. For example, Minko *et al.*[42] synthesized pH-responsive hybrid silica nanoparticles surface coated with poly(2-vinylpyridine) (P2VP) brushes. Under acidic media, protonated P2VP brushes can capture negatively charged 12 nm AuNPs *via* electrostatic interactions. The pH-driven collapse and swelling of P2VP brushes can exert control over the spatial distribution of AuNPs, leading to reversible colorimetric changes in the range of pH 3–6. However, these composite AuNP-decorated silica nanospheres become unstable under neutral or alkaline media due to the insolubility of grafted P2VP chains and loss of favorable electrostatic interactions.

To overcome this issue, specific and relatively strong thiol-AuNP covalent interactions have also been exploited to fabricate responsive AuNP assemblies by employing responsive polymer templates. Previously, we reported the synthesis of star polymers possessing 4th generation hyperbranched polyester cores and thermoresponsive PNIPAM arms by reversible addition-fragmentation chain transfer (RAFT) polymerization. After transforming terminal dithioester moieties into thiol functionalities, the core-shell type unimolecular micelles can serve as templates for the assembly of citrate-capped AuNPs.[37] Several issues remain with this approach, which are described below. Firstly, the star polymer templates possess a maximum of 64 surface-terminated thiols, which limits the number of covalently attached AuNPs; secondly, the star polymer templates are soft and less well-defined in chemical structures; finally, monothiol–Au interactions have been known to be quite weak and are subject to exchange reactions in the presence of free thiols.

Thus, it is highly desirable to employ a relatively rigid responsive template possessing stimuli-tunable dimensions and a surface attached with stronger Au-binding ligands for the covalent assembly of AuNPs. Compared to single thiol-containing ligands, it is well-known that 1,2-dithiolane moieties can strongly chemisorb and stably anchor onto AuNP surfaces.[55] Herein, we report on the fabrication of water-dispersible composite silica nanospheres covalently anchored with AuNPs possessing thermo-tunable spatial distributions at the outer periphery of thermoresponsive PNIPAM brushes (Scheme 1). Hybrid silica nanoparticles coated with 1,2-dithiolane end-capped PNIPAM brushes were synthesized at first by combining surface-initiated atom transfer radical polymerization (ATRP) and click post-functionalization techniques. Transmission electron microscopy (TEM), dynamic laser light scattering (LLS), and UV absorption measurements were conducted to verify the morphologies of AuNP-decorated composite silica nanospheres, thermo-induced collapse/swelling transitions of PNIPAM brushes sandwiched between silica nanoparticle cores and surface embedded AuNPs, and thermo-tunable spatial distributions and thermo-reversible surface plasmon absorption band shift of covalently assembled AuNPs. We envisage that the currently reported strategy of covalent assembly of AuNPs into well-defined composite nanospheres possessing thermo-tunable characteristics can be further exploited for colorimetric temperature sensing and responsive SERS detection purposes.

2. Experimental section

Materials

N-Isopropylacrylamide (NIPAM, 97%, Tokyo Kasei Kagyo Co.) was purified by recrystallization from a mixture of benzene and *n*-hexane (1/3, v/v). CuCl (99.999%), $CuCl_2$ (99%), CuBr (99.999%), NaN_3 (99%), *N*,*N*,*N*′,*N*″,*N*″-pentamethyldiethylenetriamine (PMDETA), and D,L-thioctic acid (99%) were purchased from Aldrich and used without further purification. Tetraethoxysilane (TEOS) and 3-aminopropyl-triethoxysilane (APTES) were purchased from Silicone Materials Co. (Wuhan Univ.) and distilled under reduced pressure just prior to use. Tris(2-(dimethylamino)ethyl)amine (Me_6TREN),[56] citrate-protected AuNPs with an average size of 12 nm,[35] and 2-bromoisobutyrate functionalized silica nanoparticles[57–59] were prepared according to literature procedures. All other reagents were purchased from Sinopharm Chemical Reagent Co. Ltd and used as received.

Sample preparation

General approaches employed for the preparation of hybrid silica nanoparticles coated with 1,2-dithiolane end-capped PNIPAM brushes and composite silica nanospheres surface decorated with AuNPs are shown in Scheme 1.

Synthesis of 1,2-dithiolane-3-pentanoic acid-*N*-propargylamide. 1,2-Dithiolane-3-pentanoic acid-*N*-propargylamide was synthesized through the amidation reaction of D,L-thioctic acid with a slight excess of propargylamine in the presence of *N*,*N*′-dicyclohexylcarbodimide (DCC) and 4-dimethylaminopyridine (DMAP). A typical procedure was as follows. D,L-thioctic acid (2.55 g, 12.4 mmol), DCC (3.0 g, 14.6 mmol), and DMAP (0.18 g, 1.48 mmol) were dissolved in 50 mL anhydrous CH_2Cl_2, the

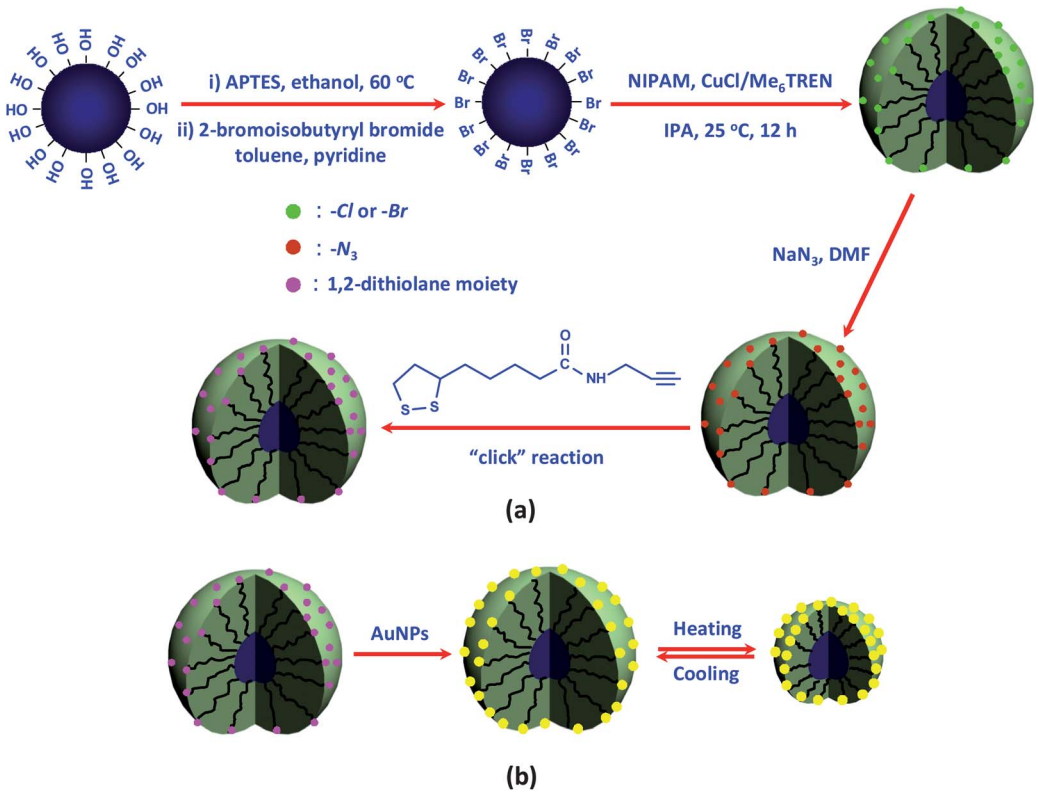

Scheme 1 Schematic illustration of (a) the synthesis of organic/inorganic hybrid silica nanoparticles surface coated with 1,2-dithiolane end-capped poly(*N*-isopropylacrylamide) (PNIPAM) brushes and (b) the fabrication of hybrid silica nanospheres anchored with gold nanoparticles (AuNPs) at the outer periphery of the thermoresponsive PNIPAM brush. The obtained SiO_2/PNIPAM brush/AuNP composite nanospheres exhibit reversible thermoresponsive swelling/collapse transitions, accompanied with the thermo-modulation of spatial distances between neighboring surface-attached AuNPs.

reaction mixture was cooled to 0 °C and propargylamine (0.80 g, 14.5 mmol) in 10 mL dry CH_2Cl_2 was added dropwise under magnetic stirring. The mixture was then stirred at room temperature for 12 h. After filtration, the solvent was removed on a rotary evaporator. The obtained crude product was purified by column chromatography on silica gel (100–200 mesh) using ethyl acetate/petroleum ether (1 : 2, v/v) as the eluent, affording ~2.4 g (~80% yield) yellow solid. ^{1}H NMR in $CDCl_3$, δ (ppm): 1.47 (m, 2H), 1.69 (m, 4H), 1.9 (m, 1H), 2.2 (m, 3H), 2.46 (m, 1H), 3.15 (m, 2H), 3.56 (m, 1H), 4.05 (m, 2H).

Surface-initiated ATRP of NIPAM from initiator-functionalized silica nanoparticles. Into a Schlenk flask equipped with a magnetic stirring bar, 2-bromoisobutyrate-functionalized silica nanoparticles (200 mg, 0.03 mmol initiator), Me_6TREN (26 mg, 0.11 mmol), $CuCl_2$ (1.3 mg, 0.01 mmol), NIPAM (4 g, 35.4 mmol), and 2-propanol (4 mL) were charged and ultrasonically dispersed. The mixture was degassed by one freeze-pump-thaw cycle followed by the addition of $CuCl_2$ (10 mg, 0.10 mmol) in the frozen state under protection of N_2 flow. The flask was then subjected to two additional freeze-pump-thaw cycles and placed in an oil bath thermostated at 25 °C. Stirring was started immediately after the thawing process. After 12 h, the reaction flask was opened, exposed to air, and the reaction mixture was diluted with 2-propanol. Hybrid nanoparticles were isolated *via* centrifugation at ~15 000 rpm for 1 h and the sediments were then washed with ethanol. The above centrifugation-washing cycle was repeated three times. The obtained hybrid silica nanoparticles coated with halogen-terminated PNIPAM brushes were dried in a vacuum oven overnight at room temperature. A portion of obtained hybrid silica nanoparticles was dispersed in THF *via* ultrasonication and etched with hydrofluoric acid (HF, 47 wt %) to cleave the surface grafted PNIPAM for subsequent GPC measurement (*Caution! HF is extremely corrosive and all operations with aqueous HF should be conducted in a fume hood with suitable personal protective equipment*).

Synthesis of hybrid silica nanoparticles coated with azide-terminated capped PNIPAM brushes. Hybrid silica nanoparticles coated with halogen end-capped PNIPAM brushes (1.0 g) and NaN_3 (0.1 g, 1.54 mmol) were dispersed in DMF (9 mL) under ultrasonication, the solution was then stirred at 100 °C for 24 h. After filtration to remove the insoluble solid, the azide-modified hybrid silica nanoparticles were separated and purified *via* repeated cycles of centrifugation and washing with ethanol. The obtained product was dried in a vacuum oven overnight at room temperature.

Synthesis of hybrid silica nanoparticles coated with 1,2-dithiolane end-capped PNIPAM brushes. Hybrid silica nanoparticles coated with 1,2-dithiolane end-capped PNIPAM brushes were

prepared *via* "click" reaction. In a typical procedure, hybrid silica nanoparticles coated with azide end-capped PNIPAM brushes (0.7 g), 1,2-dithiolane-3-pentanoic acid-*N*-propargylamide (0.1 g, 0.41 mmol), PMDETA (17 mg, 0.1 mmol), and DMF (4.0 mL) were added into a Schlenk flask equipped with a magnetic stir bar. After ultrasonic dispersion, the mixture was degassed by one freeze-pump-thaw cycle. In the frozen state, CuBr (14 mg, 0.1 mmol) was added under the protection of N_2 flow. The flask was then subjected to two additional freeze-pump-thaw cycles and placed in an oil bath thermostated at 25 °C. After 20 h, the obtained hybrid silica nanoparticles coated with 1,2-dithiolane end-capped PNIPAM chains were separated *via* repeated cycles of centrifugation and washing with ethanol. The product was then dried in a vacuum oven overnight at room temperature.

Synthesis of composite silica nanospheres covalently anchored with AuNPs at the outer periphery of PNIPAM brushes. Hybrid silica nanoparticles coated with 1,2-dithiolane end-capped PNIPAM brushes (10.0 mg) were re-dispersed in water (10 mL) under ultrasonication. The dispersion was then added into an aqueous dispersion of citrate-stabilized AuNP sols (150 mL). After equilibration for 24 h at room temperature, the mixture was subjected to centrifugation at 6 000 rpm for 3 min. After discarding the supernatant solution, deionized water was added and the above dispersion-centrifugation cycle was repeated three times. The final composite silica nanospheres were dispersed in 15 mL deionized water for further experiments.

Characterization

Molecular weights and molecular weight distributions were determined by gel permeation chromatography (GPC) equipped with a Waters 1515 pump and Waters 2414 differential refractive index detector (set at 30 °C). It used a series of three linear Styragel columns HT2, HT4, and HT5 at an oven temperature of 45 °C. The eluent was THF at a flow rate of 1.0 mL min^{-1}. A series of low polydispersity polystyrene standards were employed for the GPC calibration. Fourier transform infrared (FT-IR) spectra were recorded on a Bruker VECTOR-22 IR spectrometer. The spectra were collected at 64 scans with a spectral resolution of 4 cm^{-1}. XPS was performed using an ESCALAB-MK II instrument (VG, UK) with a monochromatic Al Kα X-ray source. Thermogravimetric analysis (TGA) was performed in air at a heating rate of 10 °C min^{-1} from room temperature to 700 °C using Perkin Elmer Diamond TG/DTA. High resolution transmission electron microscopy (HRTEM) observations were conducted on a JEOL 2010 electron microscope. The sample for HRTEM observations was prepared by spreading 10 μL nanoparticle solution onto copper grids successively coated with thin films of Formvar and carbon. No staining was required. A commercial spectrometer (ALV/DLS/SLS-5022F) equipped with a multi-tau digital time correlator (ALV5000) and a cylindrical 22 mW UNIPHASE He–Ne laser (λ_0 = 632 nm) as the light source was employed for dynamic and static LLS measurements. In dynamic LLS, scattered light was collected at a fixed angle of 90° for a duration of ~5 min. Distribution averages and particle size distributions were computed using cumulants analysis and CONTIN routines. All the data were averaged over three measurements. UV-Vis absorption spectra were with acquired on a Unico UV/vis 2802PCS spectrophotometer using a thermostatically controlled couvette.

3. Results and discussion

Surface-initiated ATRP of NIPAM from 2-bromoisobutyrate-functionalized silica nanoparticles

General strategies employed for the preparation of hybrid silica nanoparticles coated with PNIPAM brushes and composite silica nanospheres covalently decorated with AuNPs at the surface of PNIPAM brushes are shown in Scheme 1. 2-Bromoisobutyrate-functionalized silica nanoparticles with an average radius of ~45 nm as determined by HRTEM and SEM examinations (Fig. 1a and 1b; Fig. 2a) were prepared following procedures reported previously.[57,58] Typical synthetic procedures are summarized as follows (Scheme 1a). Bare silica nanoparticles prepared *via* the Stöber process were modified with APTES at first to afford primary amine-functionalized silica nanoparticles; 2-bromoisobutyrate-functionalized silica nanoparticles were then prepared *via* the amidation reaction of amine-functionalized silica nanoparticles with 2-bromoisobutyryl bromide. The

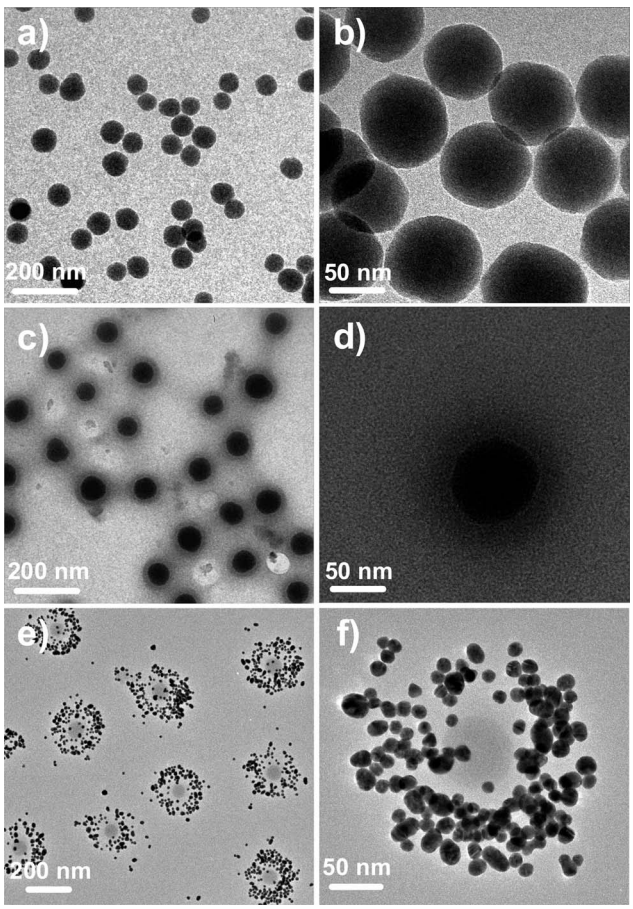

Fig. 1 HRTEM images of (a) and (b): 2-bromoisobutyrate-functionalized silica nanoparticles; (c) and (d): organic/inorganic hybrid silica nanoparticles coated with thermoresponsive PNIPAM brushes synthesized *via* surface-initiated ATRP technique; (e) and (f): composite silica nanospheres covalently anchored with AuNPs at the outer periphery of the thermoresponsive PNIPAM brush.

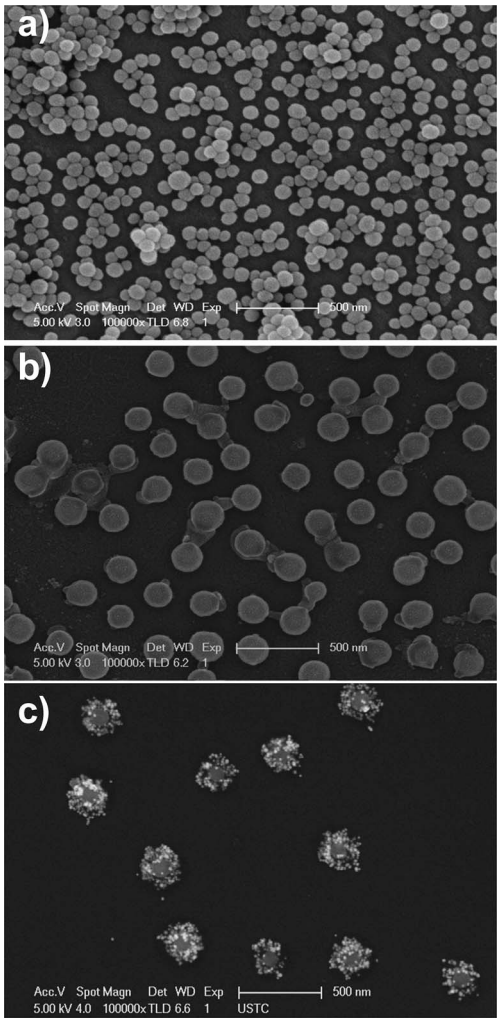

Fig. 2 SEM images recorded for (a) 2-bromoisobutyrate-functionalized silica nanoparticles, (b) hybrid silica nanoparticles coated with thermoresponsive PNIPAM brushes, and (c) composite silica nanospheres covalently anchored with AuNPs at the outer periphery of the PNIPAM brush.

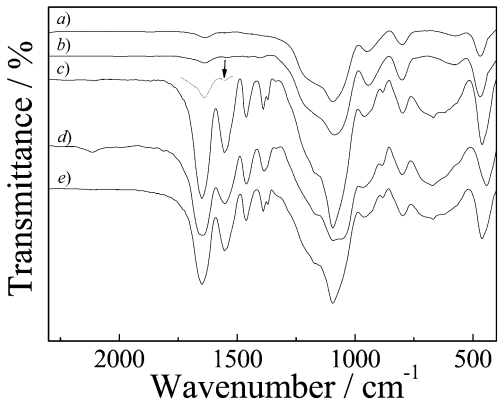

Fig. 3 Fourier transform infrared (FT-IR) spectra of (a) bare silica nanoparticles, (b) 2-bromoisobutyrate-functionalized silica nanoparticles, (c) hybrid silica nanoparticles coated with PNIPAM brushes, (d) hybrid silica nanoparticles coated with azide-terminated PNIPAM brushes, and (e) hybrid silica nanoparticles coated with 1,2-dithiolane end-capped PNIPAM brushes. The arrow indicates the amide II band (1540 cm^{-1}, N–H stretching).

product was characterized by FT-IR analysis. The presence of amide moieties can be evidenced by the appearance of a relatively weak amide II band (1540 cm^{-1}, N–H stretching) (Fig. 3b), as compared to that of bare silica nanoparticles (Fig. 3a).

The successful covalent attachment of 2-bromoisobutyrate ATRP initiating moieties at the surface of the silica nanoparticle can also be confirmed from XPS analysis, which directly reflects nanoparticle surface compositions. For bare silica nanoparticles, characteristic signals of silicon (Si2p at 103 eV and Si2s at 155 eV) and oxygen (O1s at 532 eV) are clearly visible (Fig. 4a); we can also discern a weak carbon signal (C1s at 285 eV), which might be ascribed to incomplete hydrolysis and condensation of ethoxysilyl residues during the preparation of bare silica nanoparticles. After the amidation reaction of amine-modified silica nanoparticles with 2-bromoisobutyrate, the XPS survey spectrum (Fig. 4b) reveals the appearance of characteristic signals of nitrogen (N1s at 400 eV) and bromine (Br3d at 68 eV). The relative intensity of the C1s peak also becomes higher compared to that of bare silica nanoparticles. TGA analysis reveals a ~2.0 wt% difference in weight retentions at 650 °C between amine- and 2-bromoisobutyrate-functionalized silica nanoparticles (Figure S1†). If the mass retention of amine-functionalized silica nanoparticles at 650 °C is utilized as the reference sample and the density of silica nanoparticles is assumed to be identical to that of bulk silica (2.07 g cm^{-3}), the grafting density of 2-bromoisobutyrate moieties at the surface of silica nanoparticles is estimated to be ~0.31 nm^2/initiator.

In the subsequent step, surface-initiated ATRP polymerization of NIPAM from initiator-derivatized silica nanoparticles was conducted in 2-propanol at ambient temperature using CuCl/$CuCl_2$ and Me_6TREN as the catalyst. $CuCl_2$ (10 mol% relative to CuCl) was added to ensure an efficient exchange between the dormant and active species to control the surface-initiated ATRP process.[60] GPC analysis of PNIPAM chains cleaved from hybrid silica nanoparticles *via* etching with hydrofluoric acid revealed an M_n of 64,000 and an M_w/M_n of 1.25 (Figure S2†). As a result, the degree of the polymerization (DP) of grafted PNIPAM chains is *ca.* 570. The relatively narrow polydispersity and almost symmetric GPC elution trace suggest that the surface-initiated ATRP process was conducted in a relatively controlled manner.

HRTEM images of hybrid silica nanoparticles surface-coated with PNIPAM brushes are shown in Fig. 1c and 1d. It is quite evident that the silica cores are surrounded by a shaded polymer layer with a thickness of *ca.* 30 nm. The SEM images of 2-bromoisobutyrate-functionalized and PNIPAM brush-coated silica nanoparticles exhibit similar structural features (Fig. 2a and 2b). Fig. 3c shows the FT-IR spectrum of PNIPAM brush-coated hybrid silica nanoparticles, in which the amide I band (1650 cm^{-1}, C=O stretching) and amide II band (1550 cm^{-1}, N–H stretching) can be clearly discerned. Moreover, the presence of two absorption bands with almost equal intensity at 1367 cm^{-1} and 1388 cm^{-1} is associated with the deformation mode of two methyl groups of isopropyl in NIPAM repeating units. Another

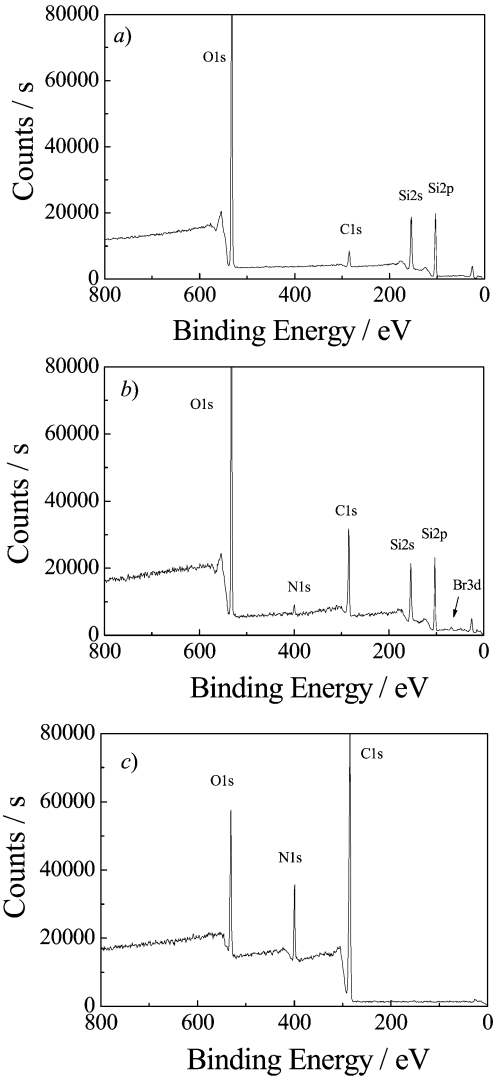

Fig. 4 XPS survey spectra of (a) bare silica nanoparticles, (b) 2-bromoisobutyrate-functionalized silica nanoparticles, and (c) hybrid silica nanoparticles coated with PNIPAM brushes.

interesting feature of PNIPAM brush-coated hybrid silica nanoparticles comes from the XPS survey spectrum (Fig. 4c). We can only observe characteristic signals of carbon, oxygen, and nitrogen in the XPS spectrum, whereas the Si signal is not detected. This indicates that silica nanoparticle cores were densely covered with a thick PNIPAM shell, and silica cores were beyond the XPS probing depth. From the TGA results (Figure S1d†), the weight retention of PNIPAM brush-grafted hybrid silica nanoparticles at 650 °C was determined to be ~33.1%. Thus, the weight fraction of PNIPAM is calculated to be ~62% when amine-functionalized silica nanoparticles are taken as a reference. In addition, by combining the TGA data and molecular weight of cleaved PNIPAM chains determined from GPC (Figure S2†), the grafting density of PNIPAM chains at the surface of silica nanoparticles is estimated to be 1.83 nm^2/chain. As the grafting density of 2-bromoisobutyrate ATRP initiating moieties at the surface of silica nanoparticles is ~0.31 nm^2/initiator, the initiating efficiency of ATRP surface grafting can be roughly estimated to be ~17%.

Synthesis of hybrid silica nanoparticles coated with 1,2-dithiolane end-capped PNIPAM brushes and composite silica nanospheres decorated with AuNPs at the surface of PNIPAM brushes

Hybrid silica nanoparticles surface-coated with 1,2-dithiolane end-capped PNIPAM chains were prepared *via* the "click" reaction (Scheme 1a). In the first step, halogen end-capped PNIPAM brushes grafted at the surface of silica nanoparticles were reacted with an excess of NaN_3, resulting in the substitution of halogen (Br or Cl) atoms with azide moieties. This was verified by the characteristic absorbance peak of azide groups at 2100 cm^{-1} in its FT-IR spectrum (Fig. 3d). Hybrid silica nanoparticles coated with 1,2-dithiolane end-capped PNIPAM brushes were then obtained *via* the "click" reaction of azide terminal groups with a slight excess of 1,2-dithiolane-3-pentanoic acid-*N*-propargylamide. The FT-IR spectrum (Fig. 3e) reveals that after the "click" reaction, the characteristic absorbance peak of azide functionalities at 2100 cm^{-1} completely disappeared, as compared to that before the "click" reaction. This partially confirms the high efficiency of the "click" reaction. Fig. 5 shows the peak-fitted S2p XPS spectra recorded for hybrid silica nanoparticles coated with azide end-capped PNIPAM brushes before and after the "click" reaction. The appearance of a S2p signal (164 eV) for hybrid silica nanoparticles after the "click" reaction further verifies the successful attachment of 1,2-dithiolane moieties at the periphery of PNIPAM brushes. If we assume 100% efficiency during the azide substitution and "click" reaction steps, we can assume that there exist ~13900 surface-terminated dithiolane moieties per hybrid nanoparticle.

In the next step, the mixing of aqueous dispersions of citrate-capped 12 nm AuNPs with hybrid silica nanoparticles coated with 1,2-dithiolane end-capped PNIPAM brushes led to the fabrication of composite silica nanospheres surface-decorated with AuNPs (Scheme 1b). Due to the strong covalent interactions between Au atoms and dithiolane moieties, AuNPs can stably anchor onto the outer periphery of hybrid silica nanoparticle templates. The interparticle cross-linking between hybrid silica nanoparticles was inhibited because the concentration of hybrid silica nanoparticles was quite low and an excess amount of AuNPs was employed. Free AuNPs can be facilely removed

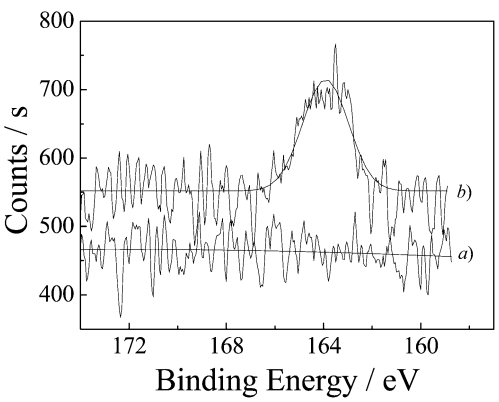

Fig. 5 Peak-fitted S2p signal of XPS spectra of hybrid silica nanoparticles coated with (a) azide-terminated PNIPAM brushes and (b) 1,2-dithiolane end-capped PNIPAM brushes.

via repeated washing-centrifugation cycles. Fig. 1e and 1f show HRTEM images of composite silica nanospheres decorated with AuNPs at the outer periphery of PNIPAM brushes. We can observe that small sized AuNPs were densely loaded around the PNIPAM shell. On average, there are ~100–120 AuNPs attached at the surface of composite silica nanospheres. SEM observations (Fig. 2c) gave further confirmative results indicating the surface covalent grafting of AuNPs.

Thermo-induced collapse/swelling of responsive hybrid silica nanoparticles surface loaded with and without AuNPs

On the basis of the average chain grafting density (1.83 nm^2/chain) estimated in the previous section, the average distance between neighboring PNIPAM chain grafting sites at the surface of silica nanoparticles can be estimated to be ~1.35 nm. Due to the hydrodynamic dimension (~8–10 nm) of free PNIPAM chains with a DP of ~570 (comparable to the chain length of grafted PNIPAM chains) being much larger than the average distance between neighboring grafted PNIPAM chains, the grafted PNIPAM layer should fall into the brush regime. PNIPAM chains in the outer brush are expected to be densely packed and forced to stretch away from the silica nanoparticle surface due to steric exclusion effects.

Dynamic LLS was then employed to characterize thermo-modulated changes in the hydrodynamic sizes of hybrid silica nanoparticles coated with dithiolane-terminated PNIPAM brushes before surface anchoring with AuNPs (Fig. 6). It is well-known that PNIPAM homopolymer chains undergo coil-to-globule phase transitions in dilute aqueous solution above the lower critical solution temperature (LCST) of *ca.* 32 °C.[61] At temperatures below the LCST, PNIPAM chains adopt a random-coil conformation; whereas at temperatures above the LCST, the hydrogen bonding interactions between water molecules and amide moieties along the PNIPAM chains are disrupted, accompanied by the chain collapse and aggregation process.[62,63] As we can observe from Fig. 6, upon heating, the intensity-average hydrodynamic radius, $<R_h>$, of hybrid silica nanoparticles coated with dithiolane-terminated PNIPAM brushes decreases monotonically from 167 to 148 nm in the temperature range of 20–29 °C, and then exhibits a further more abrupt decrease from 148 nm at 29 °C to 115 nm at 37 °C. As reported previously,[57,63] this type of two-stage thermo-induced collapsing behavior of PNIPAM brushes grafted at the surface of silica nanoparticles can be correlated with the heterogeneity in chain packing densities between inner and outer PNIPAM layers. The inner PNIPAM layer with high chain density tends to collapse at lower temperatures compared to that of the outer layer.

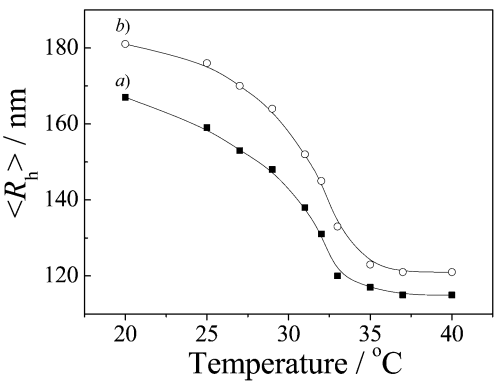

Fig. 6 Temperature dependence of intensity-average hydrodynamic radius, $<R_h>$, recorded for 5.0×10^{-5} g L^{-1} aqueous dispersion of (a) hybrid silica nanoparticles coated with dithiolane-terminated thermo-responsive PNIPAM brushes and (b) composite silica nanospheres covalently anchored with AuNPs at the outer periphery of PNIPAM brushes.

It is worthy of note that hybrid silica nanoparticles coated with dithiolane-terminated PNIPAM brushes possess a $<R_h>$ of ~167 nm at 20 °C. After surface anchoring with 12 nm AuNPs, the composite silica nanospheres exhibit a $<R_h>$ of 181 nm at 20 °C (Fig. 6). This discrepancy (~14 nm) further verified that AuNPs were anchored at the outer periphery of PNIPAM brushes. If AuNPs were embedded within the brush layer, it would basically lead to little changes or even the decrease of hydrodynamic dimensions because the nanoparticle might act as a multidentate cross-linker for the PNIPAM brush layer. This is understandable considering that AuNPs typically exhibit weak interactions with PNIPAM chains and 1,2-dithiolane-Au interactions are the dominant factor. The temperature dependence of the $<R_h>$ of composite silica nanospheres anchored with AuNPs at the outer periphery of PNIPAM brushes is also shown in Fig. 6. The $<R_h>$ of AuNP surface anchored composite silica nanospheres is systematically larger than that before AuNP surface grafting. Upon heating, $<R_h>$ of composite silica nanospheres decreases from 181 to 164 nm in the temperature range of 20–29 °C, and then exhibits a further decrease from 164 nm to 121 nm in the temperature range of 29–37 °C. The temperature-dependent dimensional changes are quite comparable to those of hybrid silica nanoparticles coated with dithiolane-terminated PNIPAM brushes. These results suggest that the surface anchoring of AuNPs at the outer surface of PNIPAM brushes does not affect the thermal phase transitions of the PNIPAM brush layer sandwiched between outer AuNPs and inner silica nanoparticle cores.

It is interesting to note that the thermo-induced collapse/swelling of PNIPAM brushes within composite silica nanospheres can spontaneously modulate the spatial distribution of surface-anchored AuNPs. UV-Vis absorption spectrometry has been proved to be a convenient and powerful technique to monitor the temperature-dependence of interparticle distances between surface-anchored AuNPs due to changes in surface plasmon absorption bands. Fig. 7 shows the UV-Vis spectra obtained at 20 °C for aqueous dispersions of citrate-stabilized AuNPs and composite silica nanospheres anchored with AuNPs. Dispersed citrate-capped AuNPs exhibit a surface plasmon absorption band with a maximum at 520 nm at 20 °C, whereas for composite silica nanospheres, they exhibit a considerably broader surface plasmon absorption peak with a maximum at ~535 nm at 20 °C. Both the red-shift of the surface plasmon absorption band and the peak broadening indicate the enhanced interparticle coupling for AuNPs covalently assembled at the surface of PNIPAM brushes. Similar phenomena were also reported for assembled AuNPs at the surface of other spherical templates.[37,42–44]

The UV–Vis absorption spectra of composite silica nanospheres surface-anchored with AuNPs were then collected at

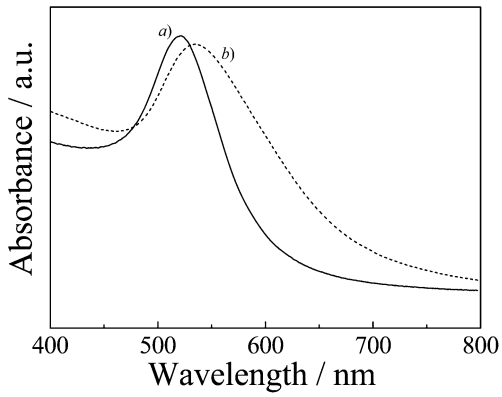

Fig. 7 UV–vis spectra recorded for the aqueous dispersion of (a) citrate-stabilized AuNPs and (b) composite silica nanospheres covalently anchored with AuNPs at the outer periphery of PNIPAM brushes.

different temperatures and the results are shown in Fig. 8, along with the temperature-dependence of surface plasmon absorption peak maxima. Upon heating, the surface plasmon absorption bands exhibited a gradual red-shift and a shoulder peak appeared at ~620 nm at elevated temperatures (Fig. 8a). Correspondingly, the surface plasmon absorption peak maxima exhibit a red-shift from 535 to 540 nm in the temperature range of 20–29 °C, and then exhibit a further shift from 540 nm to 550 nm in the temperature range of 29–37 °C (Fig. 8b), which agrees quite well with the thermo- induced two-stage collapsing behavior as determined by dynamic LLS (Fig. 6). According to thermo-induced changes of $<R_h>$ for hybrid silica nanospheres surface coated with dithiolane-terminated PNIPAM brushes in the temperature range of 20–37 °C (167 nm at 20 °C; 115 nm at 37 °C; Fig. 6), we can roughly estimate that upon heating from 20 °C to 37 °C, the interparticle distance between neighboring AuNPs exhibits a decrease of ~1.5 times. This well explains the thermo-induced red-shift of the surface plasmon absorption band due to the enhancement of interparticle coupling effects. Moreover, the thermo-induced shift of the AuNP surface plasmon bands is quite reversible. Upon cooling from 37 °C to 20 °C, the peak maxima shift back to the original position at 20 °C and this type of thermo-induced red-shift and cooling-induced peak restoration can be repeated for at least 4 cycles (Fig. 9). This is in reasonable agreement with the fact that the thermo-induced collapse/swelling of PNIPAM brushes is fully reversible.

4. Conclusions

Composite silica nanospheres covalently anchored with AuNPs possessing thermo-tunable spatial distributions at the outer periphery of thermoresponsive PNIPAM brushes were prepared *via* the template-assisted self-assembly technique. Firstly, hybrid silica nanoparticles coated with PNIPAM brushes were fabricated *via* surface-initiated ATRP from initiator-functionalized silica nanoparticles. The substitution reaction of halogen terminal groups of grafted PNIPAM brushes with sodium azide and subsequent "click" reaction with 1,2-dithiolane-3-pentanoic acid-*N*-propargylamide afforded hybrid silica nanoparticles coated with 1,2-dithiolane end-capped PNIPAM brushes. AuNPs were then covalently anchored to the outer periphery of hybrid silica nanoparticles *via* the strong interactions between dithiolane moieties and AuNPs. PNIPAM brushes at the surface of hybrid silica nanoparticles exhibit reversible thermo-induced collapse/swelling transitions, leading to the facile thermo-modulation of spatial distributions of AuNPs covalently attached at the periphery of composite silica nanospheres. It can be envisioned that composite silica nanospheres covalently anchored with AuNPs at the outer surface, which possess

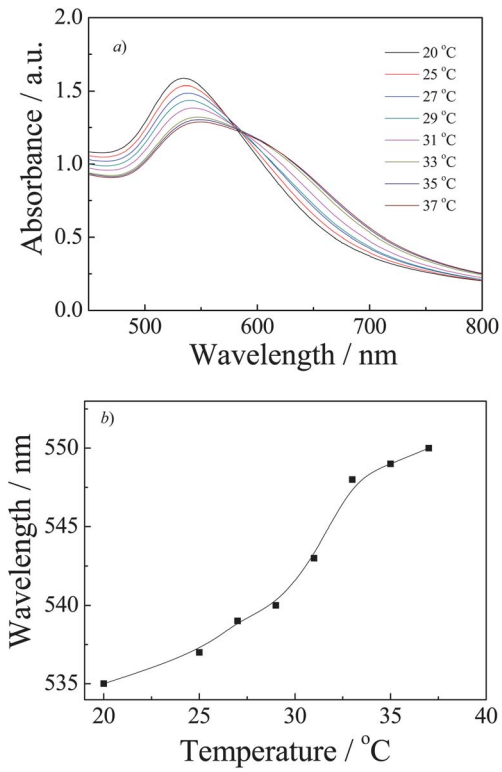

Fig. 8 Temperature dependence of (a) UV-vis spectra and (b) wavelength of surface plasmon absorption peak maxima recorded for composite silica nanospheres covalently anchored with AuNPs at the outer periphery of PNIPAM brushes. The concentration of the aqueous nanoparticle dispersion was 5.0×10^{-5} g L^{-1}.

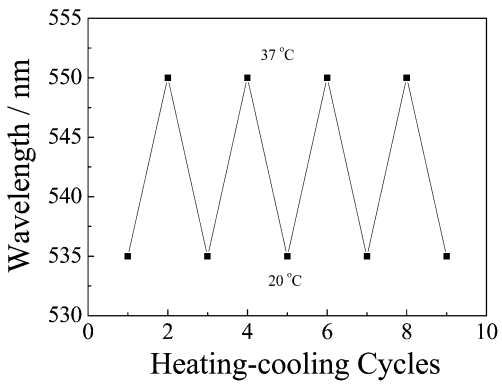

Fig. 9 Changes of the wavelength of surface plasmon absorption peak maxima of composite silica nanospheres covalently anchored with AuNPs at the outer periphery of PNIPAM brushes when subjected to the heating-cooling cycle. The concentration of the aqueous nanoparticle dispersion was 5.0×10^{-5} g L^{-1}.

thermo-tunable interparticle distances with fully reversible characteristics, could find potential applications as smart temperature sensors and responsive SERS detection matrices.

Acknowledgements

Financial support from National Natural Scientific Foundation of China (NNSFC) Projects (20874092, 91027026, 51033005, and J1030412) and Fundamental Research Funds for the Central Universities is gratefully acknowledged.

References

1 J. L. Vivero-Escoto and Y. T. Huang, *Int. J. Mol. Sci.*, 2011, **12**, 3888–3927.
2 R. Subbiah, M. Veerapandian and K. S. Yun, *Curr. Med. Chem.*, 2010, **17**, 4559–4577.
3 S. Kinge, M. Crego-Calama and D. N. Reinhoudt, *ChemPhysChem*, 2008, **9**, 20–42.
4 N. A. Kotov and S. Srivastava, *Soft Matter*, 2009, **5**, 1146–1156.
5 Z. H. Nie, A. Petukhova and E. Kumacheva, *Nat. Nanotechnol.*, 2010, **5**, 15–25.
6 V. M. Rotello, Y. Ofir and B. Samanta, *Chem. Soc. Rev.*, 2008, **37**, 1814–1823.
7 C. Sun, H. Yang, Y. Yuan, X. Tian, L. Wang, Y. Guo, L. Xu, J. Lei, N. Gao, G. J. Anderson, X.-J. Liang, C. Chen, Y. Zhao and G. Nie, *J. Am. Chem. Soc.*, 2011, **133**, 8617–8624.
8 M. H. Yang, B. G. Choi, H. Park, T. J. Park, W. H. Hong and S. Y. Lee, *Electroanalysis*, 2011, **23**, 850–857.
9 S. Peng, P. Kannan, G. Longhua, S. Hungsun and K. Dong-Hwan, *Biosens. Bioelectron.*, 2011, **26**, 3845–3851.
10 S. T. Wang, K. J. Chen, T. H. Wu, H. Wang, W. Y. Lin, M. Ohashi, P. Y. Chiou and H. R. Tseng, *Angew. Chem., Int. Ed.*, 2010, **49**, 3777–3781.
11 C. H. Li, J. M. Hu, T. Liu and S. Y. Liu, *Macromolecules*, 2011, **44**, 429–431.
12 J. Nam, N. Won, H. Jin, H. Chung and S. Kim, *J. Am. Chem. Soc.*, 2009, **131**, 13639–13645.
13 X. M. Qian, J. Li and S. M. Nie, *J. Am. Chem. Soc.*, 2009, **131**, 7540–7541.
14 S. M. Nie and S. R. Emery, *Science*, 1997, **275**, 1102–1106.
15 J. Kneipp, H. Kneipp and K. Kneipp, *Chem. Soc. Rev.*, 2008, **37**, 1052–1060.
16 M. Moskovits, *J. Raman Spectrosc.*, 2005, **36**, 485–496.
17 J. F. Berret, N. Schonbeck, F. Gazeau, D. El Kharrat, O. Sandre, A. Vacher and M. Airiau, *J. Am. Chem. Soc.*, 2006, **128**, 1755–1761.
18 B. L. Frankamp, O. Uzun, F. Ilhan, A. K. Boal and V. M. Rotello, *J. Am. Chem. Soc.*, 2002, **124**, 892–893.
19 V. M. Rotello, A. K. Boal, F. Ilhan, J. E. DeRouchey, T. Thurn-Albrecht and T. P. Russell, *Nature*, 2000, **404**, 746–748.
20 M. E. van der Boom, T. Shirman and T. Arad, *Angew. Chem., Int. Ed.*, 2010, **49**, 926–929.
21 M. S. Wong, V. S. Murthy, J. N. Cha and G. D. Stucky, *J. Am. Chem. Soc.*, 2004, **126**, 5292–5299.
22 V. M. Rotello, T. H. Galow and A. K. Boal, *Adv. Mater.*, 2000, **12**, 576–579.
23 B. A. Grzybowski, A. M. Kalsin, M. Fialkowski, M. Paszewski, S. K. Smoukov and K. J. M. Bishop, *Science*, 2006, **312**, 420–424.
24 D. Ernenwein, P. Ghosh, V. Rotello and J. Chmielewski, *J. Mater. Chem.*, 2010, **20**, 5608–5611.
25 M. Miyake, Z. Shen and M. Yamada, *J. Am. Chem. Soc.*, 2007, **129**, 14271–14280.
26 M. Yamada, Z. R. Shen and M. Miyake, *Chem. Commun.*, 2006, 2569–2571.
27 U. H. F. Bunz, K. K. Caswell, J. N. Wilson and C. J. Murphy, *J. Am. Chem. Soc.*, 2003, **125**, 13914–13915.
28 J. Czernin, H. Wang, S. T. Wang, H. Su, K. J. Chen, A. L. Armijo, W. Y. Lin, Y. J. Wang, J. Sun, K. Kamei, C. G. Radu and H. R. Tseng, *Angew. Chem., Int. Ed.*, 2009, **48**, 4344–4348.
29 M. Jiang and Z. Liu, *J. Mater. Chem.*, 2007, **17**, 4249–4254.
30 C. J. Murphy and A. Gole, *Langmuir*, 2005, **21**, 10756–10762.
31 H. Ritter, K. Isenbugel, R. Branscheid and U. Kolb, *Macromol. Rapid Commun.*, 2010, **31**, 2121–2126.
32 J. F. Stoddart, R. Klajn, M. A. Olson, P. J. Wesson, L. Fang, A. Coskun, A. Trabolsi, S. Soh and B. A. Grzybowski, *Nat. Chem.*, 2009, **1**, 733–738.
33 H. G. Cui, Z. Y. Chen, S. Zhong, K. L. Wooley and D. J. Pochan, *Science*, 2007, **317**, 647–650.
34 Z. X. Deng, X. G. Han and Y. L. Li, *Adv. Mater.*, 2007, **19**, 1518–1522.
35 K. C. Grabar, R. G. Freeman, M. B. Hommer and M. J. Natan, *Anal. Chem.*, 1995, **67**, 735–743.
36 N. J. Halas, S. L. Westcott, S. J. Oldenburg and T. R. Lee, *Langmuir*, 1998, **14**, 5396–5401.
37 H. X. Xu, J. Xu, X. Z. Jiang, Z. Y. Zhu, J. Y. Rao, J. Yin, T. Wu, H. W. Liu and S. Y. Liu, *Chem. Mater.*, 2007, **19**, 2489–2494.
38 F. E. Osterloh and H. Hiramatsu, *Langmuir*, 2003, **19**, 7003–7011.
39 T. G. Park, H. Lee and S. H. Choi, *Macromolecules*, 2006, **39**, 23–25.
40 L. R. Sita, R. W. Zehner, W. A. Lopes, T. L. Morkved and H. Jaeger, *Langmuir*, 1998, **14**, 241–244.
41 H. Yan, J. P. Zhang, Y. Liu and Y. G. Ke, *Nano Lett.*, 2006, **6**, 248–251.
42 S. Minko, R. Lupitskyy and M. Motornov, *Langmuir*, 2008, **24**, 8976–8980.
43 A. Wei and B. Sadtler, *Chem. Commun.*, 2002, 1604–1605.
44 Y. D. Yin, Z. D. Lu, J. Goebl and J. P. Ge, *J. Mater. Chem.*, 2009, **19**, 4597–4602.
45 V. M. Rotello, B. L. Frankamp and A. K. Boal, *J. Am. Chem. Soc.*, 2002, **124**, 15146–15147.
46 C. D. Mao and Y. Chen, *Small*, 2008, **4**, 2191–2194.
47 A. Verma, S. Srivastava and V. M. Rotello, *Chem. Mater.*, 2005, **17**, 6317–6322.
48 B. L. Frankamp, A. K. Boal and V. M. Rotello, *J. Am. Chem. Soc.*, 2002, **124**, 15146–15147.
49 J. M. Hu and S. Y. Liu, *Macromolecules*, 2010, **43**, 8315–8330.
50 J. Xu and S. Y. Liu, *Soft Matter*, 2008, **4**, 1745–1749.
51 D. Suzuki and H. Kawaguchi, *Langmuir*, 2006, **22**, 3818–3822.
52 D. Suzuki and H. Kawaguchi, *Langmuir*, 2005, **21**, 8175–8179.
53 J. Li, W. D. He and X. L. Sun, *J. Polym. Sci., Part A: Polym. Chem.*, 2007, **45**, 5156–5163.
54 K. H. Bae, S. H. Choi, S. Y. Park, Y. Lee and T. G. Park, *Langmuir*, 2006, **22**, 6380–6384.
55 B. C. Mei, K. Susumu, I. L. Medintz and H. Mattoussi, *Nat. Protoc.*, 2009, **4**, 412–423.
56 M. Ciampolini and N. Nardi, *Inorg. Chem.*, 1966, **5**, 41–44.
57 T. Wu, Y. F. Zhang, X. F. Wang and S. Y. Liu, *Chem. Mater.*, 2008, **20**, 101–109.
58 T. Wu, G. Zou, J. M. Hu and S. Y. Liu, *Chem. Mater.*, 2009, **21**, 3788–3798.
59 T. Wu, Z. S. Ge and S. Y. Liu, *Chem. Mater.*, 2011, **23**, 2370–2380.
60 J. B. Kim, W. X. Huang, M. D. Miller, G. L. Baker and M. L. Bruening, *J. Polym. Sci., Part A: Polym. Chem.*, 2003, **41**, 386–394.
61 H. G. Schild, *Prog. Polym. Sci.*, 1992, **17**, 163–249.
62 Z. Ahmed, E. A. Gooding, K. V. Pimenov, L. L. Wang and S. A. Asher, *J. Phys. Chem. B*, 2009, **113**, 4248–4256.
63 J. Shan, J. Chen, M. Nuopponen and H. Tenhu, *Langmuir*, 2004, **20**, 4671–4676.